Journal of Chemical and Petroleum Engineering (JChPE)

Print ISSN: 2423-673X Online ISSN: 2423-6721

CFD Study of Calibration Factor for Cross Correlation Based Ultrasonic Flowmeter at Different Upstream Pipe Lengths

Mohammad Amin Alaeddin, Seyed Hassan Hashemabadi *

1. Computational Fluid Dynamics (CFD) Research Laboratory, School of Chemical, Petroleum and Gas Engineering, Iran University of Science and Technology, Tehran, Iran. E-mail: amin.alaedin@gmail.com
2. Flow Measurement Research Center, Iran University of Science and Technology, Tehran, Iran. E-mail: hashemabadi@iust.ac.ir

ARTICLE INFO

Article History:
Received: 23 August 2021
Revised: 16 March 2022
Accepted: 02 April 2022

Article type: Research

Keywords:
Accuracy,
Computational Fluid Dynamics (CFD) Simulation,
Calibration Factor,
Ultrasonic Cross-Correlation Flowmeter,
Upstream Straight Pipe Length

ABSTRACT

Despite lots of research on transit-time and Doppler flowmeter technologies, little research has been done on ultrasonic cross-correlation flowmeter technology. Since the mechanism of the ultrasonic cross-correlation flowmeter (UCCF) differs from other ultrasonic flowmeter technologies, it strongly requires individual investigations. The upstream straight pipe length is an important item that strongly affects the UCCF accuracy. Determination of proper calibration factors concerning upstream pipe length could incredibly improve the measurement precision. In the present study, the computational fluid dynamics (CFD) simulation was conducted, and the water flow inside a pipe without any flow disturbances (e.g., valve, fitting, or bend) was simulated to investigate the calibration factor for the UCCF at different upstream straight pipe lengths and different Reynolds numbers (from 76,600 to 383,400). For accurately predicting the turbulent flow behavior, Reynolds Stress Model (RSM) was used in this study. The results indicated that by increasing the upstream pipe length up to approximately 25 times pipe diameter, the required calibration factor decreases, then increases, and finally remains constant at lengths greater than 40 times pipe diameter. Eventually, a proper correction factor on the calibration curve was developed at different flow Reynolds numbers, for the first time, to modify the calibration curve at various upstream pipe lengths.

Introduction

The accuracy of the flowmeter is counted as the most important parameter in measurement processes, especially in the custody transfer field. Since petroleum products are expensive, the monetary losses due to incorrect measurement could be impressive [1]. In this manner, improvement of the flowmeter accuracy is one of the essential research topics in the field of the oil and gas measurement industry [1, 2].

Venturi, orifice plate, and ultrasonic flowmeters are different technologies that are used for single-phase flow measurement [1, 3]. The ultrasonic flowmeters are the priority because of the various benefits such as high precision, no friction loss, and no moving parts [1–4]. Ultrasonic measurement technologies are mainly categorized into three types transit-time, Doppler, and

* Corresponding Author: S. H. Hashemabadi (E-mail address: hashemabadi@iust.ac.ir)

Journal of Chemical and Petroleum Engineering, 2022, 56(1): 133- 152.
Publisher: University of Tehran, College of Engineering *DOI: 10.22059/JCHPE.2022.329324.1358*

cross-correlation [1, 5]. The main advantage of cross-correlation technology over two other technologies is performance independence from the speed of sound [1, 6–8]. The cross-correlation flowmeter sensors are clamped on the external surface of the pipe so that the sensors are not directly in contact with the flowing liquid. Therefore, these flowmeters are one the best candidates for corrosive services [1, 9].

As demonstrated in Fig. 1, the main concept of the ultrasonic cross-correlation flowmeter (UCCF) is calculating the delay time. The delay time for the UCCF is defined as the time it takes the flow to traverse the distance between the upstream and downstream sensors. One of the main differences between the UCCF and the other ultrasonic flowmeters, such as transit-time flowmeter is the sensors' circumferential arrangement on the pipe. In UCCF, the sensors are placed as opposed, while in other types, the sensors are installed diagonally on the pipe (Fig. 1) [1]. During the measuring process, both the upstream and downstream sensors send acoustic waves across the pipe to the receiver sensors on the other side of the pipe. By performing the mathematical cross-correlation function in Eq. 1 on recorded signals from the upstream and downstream sensors, the delay time is determined. The cross-correlation function is defined as follows [1, 6, 10, 11]:

$$R_{XY}(\tau) = \frac{1}{T}\int_{0}^{T} X(t-\tau)Y(t)dt \tag{1}$$

where $X(t\text{-}\tau)$and $Y(t)$ are the generated signals in sensors. Concerning Eq. 1, at different time shifts, both recorded signals are shifted relative to each other and their similarities are continuously checked. When the shifted signals have the highest degree of similarity, that time shift is noted as the UCCF delay time τ^*. The delay time is the time that takes the flow markers to travel the distance between the upstream and downstream sensors. In other words, the flow markers observed upstream will be observed downstream after the delay time [1, 6, 10]. As displayed in Fig. 1, R_{xy} function is maximum at the delay time τ^* which indicates the most conformity between upstream and downstream recorded signals [1, 6, 10].

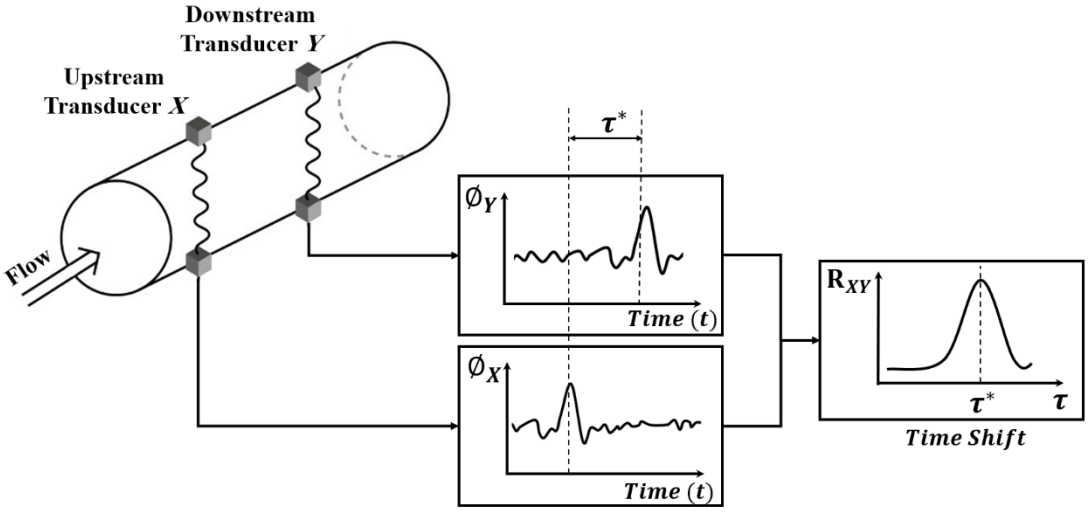

Fig. 1. The UCCF performance schematic [1]

Using the delay time (τ^*) and the axial separation distance between transducers (Δx), the convection velocity is calculated by [1, 10,12]:

$$U_{convection} = \frac{\Delta x}{\tau^*} \tag{2}$$

Convection velocity in Eq. 2 is mainly related to eddies motion velocity. When the acoustic wave is transmitted across the pipe section, the eddies in turbulent flow interact with the acoustic waves and produce fluctuating signals in receivers. These generated fluctuating signals are representative of eddies' motion through the pipe. In other words, the UCCF keeps the eddies under observation and determines eddies' velocity ($U_{Covnection}$) [1, 7, 11]. In the present study, the mathematical model of UCCF was used to calculate the delay time and the convection velocity in Eq. 2.

Since the bulk velocity is the primary purpose of measurement processes, an important parameter is defined in Eq. 3 for the UCCF, which connects the eddies convection velocity to the bulk velocity [1,10, 12]:

$$K = \frac{U_{Bulk}}{U_{Convection}} \tag{3}$$

where calibration factor (K) is the function of the axial distance between sensors [7, 12, 13], pipe roughness [12], sensors arrangement on the pipe [1, 14], and the upstream straight pipe length [15, 16].

A straight pipe means no flow disturbance (e.g., valve, fitting, and bend) on the pipe section. The existence of a fitting, bend, or valve upstream of the flowmeter causes asymmetry, swirl, and disturbed flow profile inside the pipe which leads to measurement error [16]. Therefore, concerning the ISO-12242 and API MPMS 5.8 standards recommendation, a sufficiently long straight pipe is considered to eliminate the influence of upstream disturbances and velocity profile distortion on flowmeter function and also to reduce the measurement error [15, 16]. But, due to piping limitations and space constraints in industrial plants, increasing the flowmeter upstream pipe length is not always feasible [1, 5, 14, 17]. The effect of each mentioned flow disturbance could be a fantastic subject to be investigated for future studies.

Regardless of any flow disturbances on the pipe such as valve, fitting, or bend, the straight pipe length singly is an important parameter that strongly affects the flowmeter accuracy, even in uniform and non-disturbed flow profiles. The upstream pipe length shows its effect on velocity profile evolution through the pipe. Since the velocity profile changes along the pipe length, installation of the flowmeter at different locations (or equally different upstream straight pipe lengths) causes the flowmeter observes different velocity profiles which leads to different measurement results.

Regarding the above explanations, since the flowmeter accuracy is highly dependable on upstream pipe length, using the proper calibration factor in terms of flowmeter position enhances the measurement accuracy. Therefore, it is valuable to study the influence of upstream straight pipe length on the flowmeter operation and also to provide the proper calibration factor concerning upstream pipe length.

Initially, Coulthard introduced the ultrasonic cross-correlation flowmeter to the world [6]. He tried to provide UCCF calibration curves at different generated signal amplitudes. Moreover, He realized that due to transducer arrangements in UCCF, the sound velocity does not influence the measurement accuracy. Afterward, Beck studied the flowmeter signal processing operation and demodulation methods [10]. Furthermore, he introduced flow profile, time lag, and sensor phase error factors to UCCF correlation to increase the measurement accuracy. After a while, Worch tried to define a theoretical formula for a description of the acoustic wave interaction with markers in turbulent flow based on experimental setup results.

Moreover, he studied the effect of different pipe materials on wave propagation and measurement error. The results demonstrated that in UCCF, the pipe material has a negligible effect on measurement error [8]. With the aid of experimental setup results, Schneider et al. generated the first mathematical model of the UCCF velocity measurement to connect the delay time in the UCCF model to flow bulk velocity concerning turbulent flow properties. The results showed about a 4% deviation from experimental data. Furthermore, they studied the flowmeter

performance at different sensors' axial separation distances. They showed that the measurement accuracy decreased with increasing sensor separation distance [7]. After a decade, an applicable and more rigorous mathematical flowmeter model was developed by Lysak et al. to accurately estimate the time delay measured by the UCCF. Since the previous model was developed based on a uniform power-law velocity profile, they improved the model based on turbulent flow properties.

Moreover, they presented the calibration factor for the UCCF for the flows with high Reynolds numbers using numerical simulation. Also, they studied the effect of the pipe wall roughness and axial separation distance between sensors pair on the performance of the UCCF [11, 12]. Gurevich et al. introduced a theoretical method for the generation of the turbulent field to extract turbulence data to analyze the flowmeter operation at different operating conditions [13]. Recently, Ton developed a new technique for the flowmeter function concerning his knowledge of various plants. He presented situations in which the flowmeter function is stable and accurate [18]. Newly, Alaeddin et al. investigated the performance of the UCCF at different sensor configurations for non-homogenous flow profiles [1]. They optimized the arrangement of the transducer in a multipath flowmeter using CFD simulation with a stress-omega turbulence model. The results showed a maximum 5% deviation from numerical and experimental data.

The purpose of the present investigation is to study the ultrasonic cross-correlation function at different upstream straight pipe lengths without consideration of flow disturbances on the pipe and also to develop a correction factor on the calibration curve to modify the calibration curve concerning upstream pipe length for the first time.

Numerical Study

To perform CFD simulations, the finite volume method (FVM), second-order upwind for the discretization of turbulent parameters, momentum equations, and SIMPLE algorithm for pressure-velocity coupling has been used in the present work.

Computational Domain

As displayed in Fig. 2, a smooth pipe (zero roughness) size 6 -inch- was selected with a total length of 85 times pipe diameter (85*D*) to assure that the flow reaches the hydrodynamic fully-developed length inside the pipe. The specified total length has been checked with practical equations made on the calculation of a fully developed region [19]. In the present study, the flowmeter is located at different distances of 10D, 20D, 25D, 30D, 40D, 50D, 60D, 70D, and 80D from the pipe inlet to study the influence of different upstream straight pipe lengths on the UCCF performance. Due to the symmetrical geometry and symmetrical profile of liquid flow inside the pipe, the 2D axisymmetric approach was used in the present study to reduce the computational efforts. Boundary conditions will be discussed in boundry conditions section. As displayed in Fig. 2, *L* represents the distance between the flowmeter position (first transducer) and the pipe entrance, in other words, *L* represents the upstream straight pipe length.

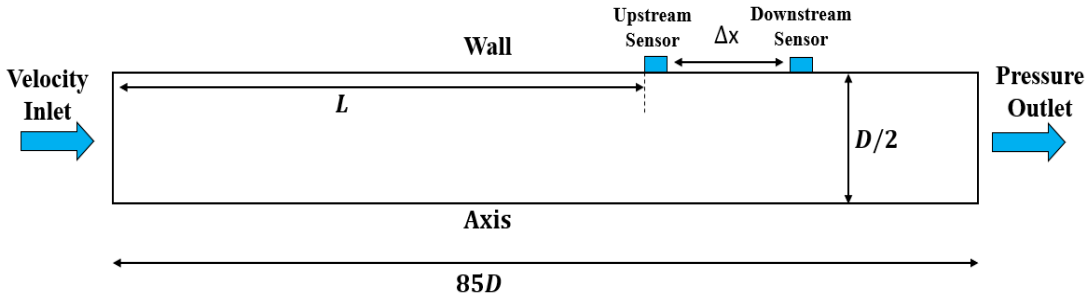

Fig. 2. The geometry of the present study and the boundary conditions

Numerical Method

The continuity and momentum equations (Eq. 4 and Eq. 5, respectively) are solved for incompressible liquid flow under steady-state conditions [20]:

$$\frac{\partial u_i}{\partial x_i} = 0 \tag{4}$$

$$\frac{\partial}{\partial x_j}\left(\rho u_i u_j\right) = -\frac{\partial p}{\partial x_i} + \frac{\partial}{\partial x_j}\left[\mu\left(\frac{\partial u_i}{\partial x_j} + \frac{\partial u_j}{\partial x_i}\right)\right] + \frac{\partial}{\partial x_j}\left(-\rho\overline{u_i' u_j'}\right) \tag{5}$$

The kinetic energy dissipation rate ε equation is as follows:

$$\frac{\partial\left(\rho\varepsilon u_i\right)}{\partial x_i} = \frac{\partial}{\partial x_j}\left\{\left(\mu + \frac{\rho C_\mu \frac{k^2}{\varepsilon}}{\sigma_\varepsilon}\right)\frac{\partial\varepsilon}{\partial x_j}\right\} + \frac{1}{2}C_{\varepsilon 1}\left[P_{ii} + C_{\varepsilon 3}G_{ii}\right]\frac{\varepsilon}{k} - C_{\varepsilon 2}\rho\frac{\varepsilon^2}{k} \tag{6}$$

Also, the simple equation for turbulent kinetic energy k is as follows:

$$k = \frac{1}{2}\overline{u_i' u_i'} \tag{7}$$

where P_{ii} denotes stress production term, G_{ii} denotes buoyancy effect, u_i' is fluctuation component of velocity and $-\rho u_i' u_j'$ represents Reynolds stress tensor. $C_{\varepsilon 1}$, $C_{\varepsilon 2}$, $C_{\varepsilon 3}$, C_μ, and σ_ε are the constants of the equations. Providing all the details of transport equations for Reynolds stresses is beyond the scope of this study and it is referred to the relevant reference [20].

The Reynolds stress model (RSM) was selected to predict the flow behavior with higher accuracy. The main reason for using RMS, besides its many strengths is that this model is the most elaborate model among the RANS turbulence model which generally predicts the turbulent parameters (such as turbulent dissipation rate ε, which is challenging and directly used in the UCCF model) more precise than other simpler RANS models. A lot of numerical research has been done on the simulation of turbulent flow. Most of them suggested that the RSM works better than eddy viscosity models in precisely predicting turbulent flow behavior [21–23]. In the present study, Linear Pressure-Strain Model was adapted for pressure-strain modeling. It is noticeable that in the RSM turbulence model, turbulent kinetic energy k is calculated based on Reynolds stresses $u_i' u_j'$ and mainly no specific transport equation is required for the determination of turbulent kinetic energy [20].

The Concept of the Flowmeter Model

The UCCF model proposed by [11, 12] has been used to calculate the delay time. Since the phase shift of the transmitted ultrasonic wave is strongly influenced by velocity fluctuations in turbulent flow, the focus of the selected model is on mathematically relating the phase shift of the transmitted ultrasonic wave to the perturbation of velocity by using the main properties of the turbulent flow [11, 12].

In the UCCF performance model, statistics of velocity perturbation were modeled along the acoustic path in terms of turbulent flow statistical properties, using spatial correlations and the spectral characteristics of turbulent flow [1,11, 12]. By stochastic predicting the velocity fluctuations along the acoustic path, the phase shift of the transmitted ultrasonic wave is well determined in terms of turbulent flow main parameters. It is out of the purpose of the present work to discuss all the details. This paper focuses on studying the flowmeter performance at different upstream straight pipe lengths with the aid of the selected UCCF model. Therefore, relevant references have found a huge volume of equations, derivations, and signal processing aspects of the UCCF model [11, 12].

Since the calculations were complex, two simplifications in the model were presented below:

1. Turbulence convection between both of the sensors is assumed to be frozen. According to this assumption, the decay or self-distortion of turbulence structures is considered negligible, and the turbulence markers travel with constant velocity [11]. This assumption works best for a short separation length between sensors [8, 11]. The separation distance between sensors was assumed $\frac{\Delta x}{D} = 1$ with respect to similar researches in UCCF field [1, 7, 12, 13] to assure proper performance of the flowmeter model.

2. The isotropic turbulence field is assumed through the computational domain. This hypothesis mainly produces reasonable results [1, 11, 24].

In the flowmeter model reference, after modeling the phase shift of the transmitted ultrasonic waves concerning the turbulent flow parameters, the mathematical cross-correlation function was expressed as follows [1, 11, 12]:

$$R_{12}(\tau) = \overline{\phi_1(t)\phi_2(t+\tau)} = \frac{1}{T}\int_0^T \phi_1(t)\phi_2(t+\tau)dt \tag{8}$$

where ϕ_1 and $\phi_2$are the phase angle of sensors *X* and *Y* in Fig. 1.

As previously described for Eq. 1 and Fig. 1, the output of Eq. 8 is the delay time that is used for the determination of the eddies' convection velocity in Eq. 2.

In the UCCF reference model, for simplification, the cross-correlation function in the model has been transferred from the time domain to the frequency domain. The final equation of the cross correlation function was expressed as follows [12]:

$$G_{12}(f) = 7.4\frac{\omega_0^2}{c_0^2}\int_0^D \frac{v^2 L_{11}^2}{U}\left[\frac{\left(f_e^2+\frac{11}{3}f^2\right)\left(f_e^2+\frac{8}{3}f^2\right)}{\left(f_e^2+\frac{8}{3}f^2\right)\left(f_e^2+f^2\right)}\right]\left[1+(\frac{f}{f_e})^2\right]^{-8/6}\exp\left(-i\,2\pi f\,\frac{\Delta x}{U}\right)dy \tag{9}$$

$$L_{11} = 0.39\frac{k^{3/2}}{\varepsilon},\quad v = \sqrt{(2/3)k},\quad f_e \approx 0.12\frac{U}{L_{11}}$$

At each specified location of the flowmeter in computational domain section (distances of *L/D* =10, 20, 25, 30, 40, 50, 60, 70 and 80 from pipe inlet), one pipe diameter $\left(\frac{\Delta x}{D}=1\right)$ is considered for the axial separation distance between transducers, which results in the most trustable outcomes for the flow measurement concerning 30 years of experience in industrial plants [18]. Similar investigations specified the same separation length Δx [7, 12, 13]. Logically, when the axial separation between sensors increases, the turbulence markers distribution change more in flow direction [1, 7, 9]. Because of this reason, at a longer separation distance between transducers, the degree of the resemblance between the recorded signals is reduced, which leads to inexact results. Extra reduction in sensor axial separation distance leads to a clash between sensor bodies that should be forbidden [1, 7]. Incidentally, the frozen hypothesis in UCCF model assumptions is endorsed especially in short axial spacing between sensors [1, 11, 13].

In described UCCF performance model, to calculate the delay timeτ^*, the distribution of turbulent dissipation rate (ε), the axial velocity (U), and the turbulent kinetic energy (k) are required along the acoustic beam path to be fed into Eq. 9.

Using the CFD simulation, the values U, k, and ε are predicted throughout the computational domain. At the pipe section where the flowmeter is placed (different distances of *L/D*), the profiles of U, k, and ε along the straight line (ultrasonic beam path) across the pipe section are extracted from the CFD simulation and are directly imported into Eq. 9.

As previously explained in the introduction, to calculate delay timeτ^*, the peak of the cross-correlation function G_{12} (f) in the time domain indicates the delay time τ^*[1, 6, 10]. Using the calculated delay time $\tau^*$and the axial distance between the two transducers (Δx), the convection velocity is calculated according to Eq. 2.

Boundary Conditions

According to Fig. 2, the pipe entrance was specified as a velocity inlet, and the outlet section was considered a pressure outlet. The selection of these boundary conditions is based on the purpose of the present work.

As discussed in the introduction, since the purpose of the present work is to investigate the effect of only upstream pipe length on flowmeter performance at different flow Reynolds numbers with uniform velocity profile without any flow disturbances the upstream of the flowmeter (e.g. valve, fitting or bend), velocity inlet boundary condition provide the proper conditions to have completely uniform velocity profile inside the pipe as expected and also makes it possible to achieve desired flow Reynolds numbers as specified in Table 1.

With the geometry and boundary conditions are shown in Fig. 2, as wished, only the pipe length becomes the critical parameter that affects the velocity profile evolution inside the pipe and the flowmeter performance. Therefore, with specified boundary conditions and selected geometry, the influence of upstream pipe length could be purely investigated.

Due to symmetrical geometry relative to the pipe axis (centerline), the axis boundary condition has been used to reduce the volume of calculations. In addition, the no-slip boundary condition for the walls has been considered.

The flow medium for this study is the water, of which the density is 998.2 kg.m$^{-3,}$ and the dynamic viscosity is 0.001 kg. (m^{-1}.s^{-1}) at the standard temperature of 15.6˚C [19].

In the present study, the calibration tests were carried out at five various flowrates which were mentioned in Table 1. The maximum allowable flow rate for the flowmeter is mainly dictated by the vendors. But in case having no information from the vendors, the maximum allowable fluid velocity inside the pipe specified by the standards and design specifications, could be counted as the secondary criterion [1]. According to NIOEC-SP-00-50, Iranian design criteria for oil and gas industries [25], in the present investigation, the velocity of 2.5 m/s was considered as the maximum velocity for calculation of maximum volumetric flow rate ($q_{V,\max}$).

The other volumetric flow rates are calculated based on $q_{V,max}$. In this regard, the flow Reynolds number in the present study varies from 76,700 to 383,400.

It is important to mention that for the determination of the calibration factor in Eq. 3, the average velocity is determined based on numerical simulation outcomes and the convection velocity is calculated by the procedure presented before. The most important operational parameters for evaluating the performance of the flowmeter at different upstream pipe lengths were given in the following table.

Table 1. Governing conditions in present work

Specification	Value
Medium Fluid	Water
Dynamic Viscosity [kg/(m·s)]	0.001 @ 15.6 ˚C.
Density (kg/m^3)	998.2
Normalized Vol. Flowrate $q_v/q_{v,\,max}$ (-)	0.2, 0.4, 0.6, 0.8 and 1
Reynolds number (-)	76,700 to 383,400
Max. allowable velocity (m/s)	2.5
Normalized Flowmeter location L/D (-)	10, 20, 25, 30, 40, 50, 60, 70, 80
The axial distance between two sensors Δx/D (-)	1

Results and Discussion

Grid Sensitivity Study

Computation runtime is mainly affected by the quantity and the structure of cells in the computational grid [1, 26]. As shown in Fig. 3, the designed mesh for the case with maximum flow rate is perfectly structured. Due to the high-velocity gradient near the wall, the grid dimensions in this area are smaller in comparison with the size of the grids in the center region of the pipe. The value of Y^+ is also maintained approximately in the range of 30 to 300 near the wall based on the standard wall function and Reynolds stress turbulence model. Fig. 4 shows the mesh independency on velocity profile at the pipe outlet. The results show that increasing the grid size to more than 88,400 has no significant effect on the outlet velocity for the case with maximum flow rate. The mesh for other cases was generated to grid size for the case with maximum flow rate.

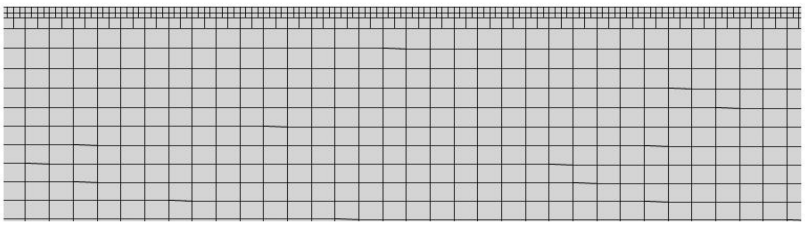

Fig. 3. Generated mesh grid for the case with maximum flowrate

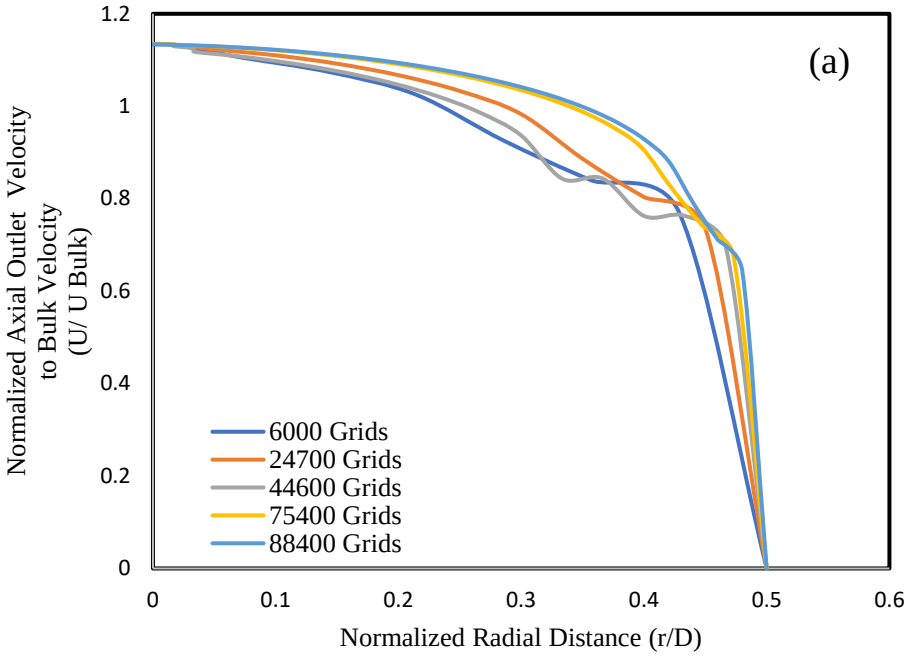
(a)
Normalized Axial Outlet Velocity to Bulk Velocity (U/ U Bulk)
Normalized Radial Distance (r/D)
6000 Grids
24700 Grids
44600 Grids
75400 Grids
88400 Grids
0
0.2
0.4
0.6
0.8
1
1.2
0.1
0.3
0.5

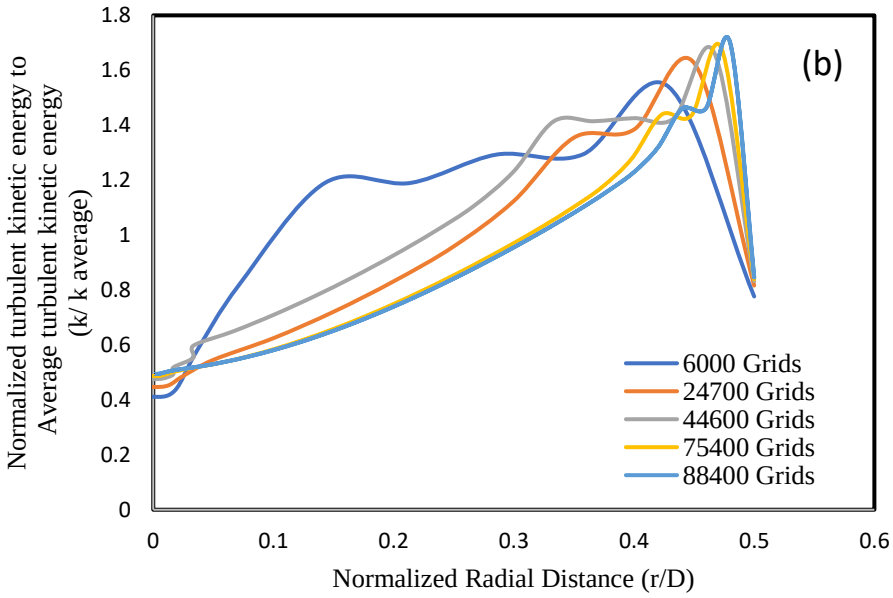
(b)
Normalized turbulent kinetic energy to Average turbulent kinetic energy (k/ k average)
Normalized Radial Distance (r/D)
6000 Grids
24700 Grids
44600 Grids
75400 Grids
88400 Grids
0
0.2
0.4
0.6
0.8
1
1.2
1.4
1.6
1.8
0.1
0.3
0.5

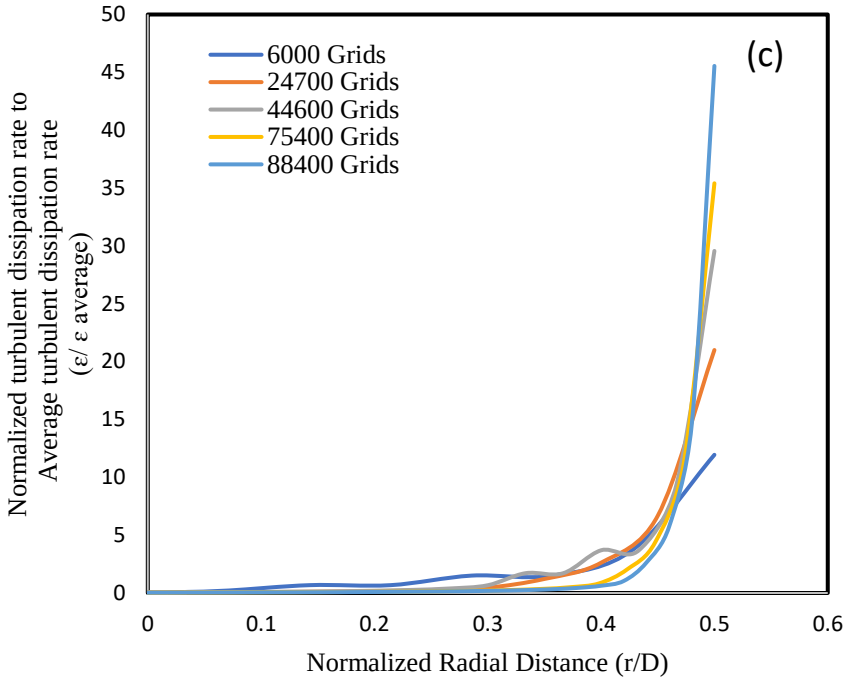

Fig. 4. Independency of results from grid size (for the case with maximum flow rate) on **(a)** Axial outlet velocity profile, **(b)** Turbulent kinetic energy profile across the beamline, **(c)** Turbulent dissipation rate profile across the beamline

Numerical Validation

For validation of the numerical procedure, a straight 4-inch- pipe with a length of 90D was considered similar to the reference geometry, and the flow with the Reynolds number range of 26×10^3 to 240×10^3 inside the pipe was simulated using the Reynolds stress turbulence model [7]. Employing the procedure presented in the concept of the flowmeter model section, the calibration factor was determined. The results are plotted in Fig. 5. The average deviation of results is about 5%. In the case of reality (experimental data), due to the turbulent structures' self-distortion, the eddies' distribution/convection change and they traverse with various convection velocities in an axial direction [7]. Since the UCCF highly responds to eddies convection velocity, decay of turbulences leads to different measurement results in comparison with the case in which the eddies frozen pattern is assumed. Therefore, the frozen assumption in the UCCF model could cause deviation from experimental data.

The development of the UCCF model is based on the turbulence energy spectrum. The energy spectrum for the turbulent stream is divided into three zones dissipation range, inertial subrange, and large-scale range [11]. The isotropic assumption is more valid in the inertial subrange of the turbulent energy spectrum. But, in a large-scale or dissipation range, where the turbulent is not isotropic, this assumption declines the UCCF model performance [11, 24]. Therefore, the isotropic assumption also could cause deviation from experimental data.

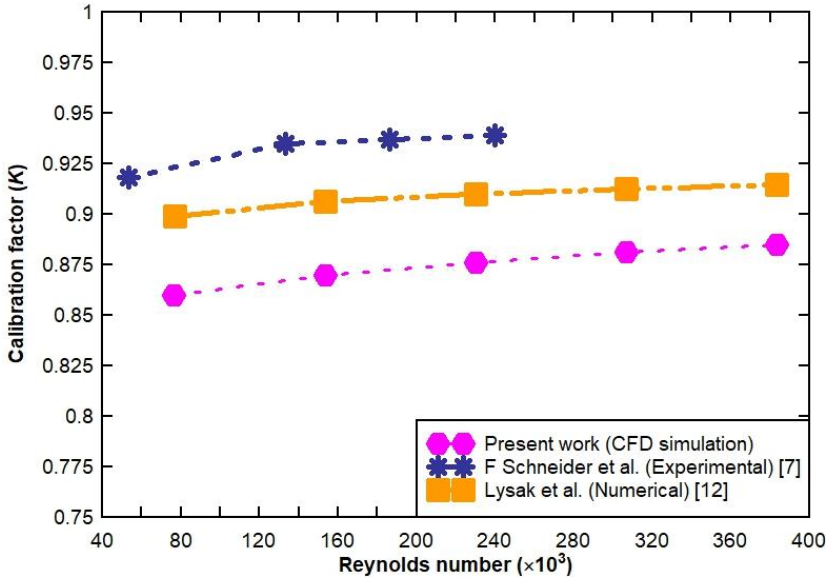

Fig. 5. Validation of CFD simulation calibration factor against experimental and numerical data [7, 12]

Fig. 5 shows the dependency of the calibration factor on the Reynolds number. The results depict that when the flow Reynolds number rises, the velocity distribution at the pipe section becomes fuller as well as at the center region of the pipe (core region). Therefore, at higher Reynolds numbers, the velocity ratio at the core region to the bulk velocity decreases. Since the convection velocity that is computed by the UCCF is mainly dependent on the center region velocity (pipe mid-section), in a flatter velocity distribution, the convection velocity reduces. Consequently, the calibration factor rises respecting to Eq. 3 [1, 12].

Another validation of the velocity profile has been done against the power-law velocity profile (Eq. 10) [19]. As illustrated in Fig. 6, the CFD simulation results align with the power-law velocity profile.

$$U = U_{\max}\left(1-\frac{r}{R}\right)^{1/7} \tag{10}$$

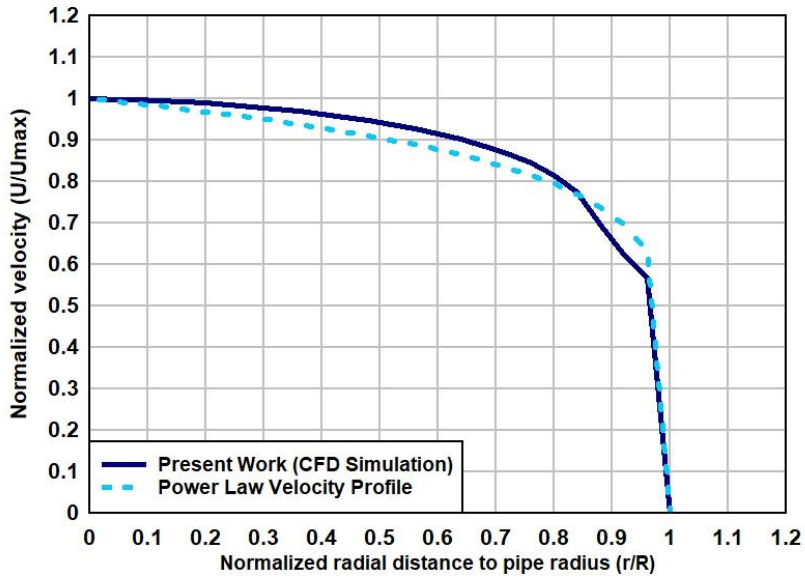

Fig. 6. Validation of velocity profile against power-law velocity profile equation

Numerical Results of the UCCF

Fig. 7 illustrates the required calibration factor for the UCCF at nine different flowmeter locations on the pipe and various fluid Reynolds numbers. Noticing Fig. 7, the UCCF calibration factor (*K*) is intensively affected by flowmeter upstream straight pipe length. For each location of the flowmeter (*L/D*), a specific calibration curve is required. Carefully noticing Fig. 7, it is obvious that for distances approximately larger than *L/D* ≥40, the calibration curves do not change significantly. Therefore, a unique calibration curve could be applicable for the flowmeter at distances greater than *L/D*=40.

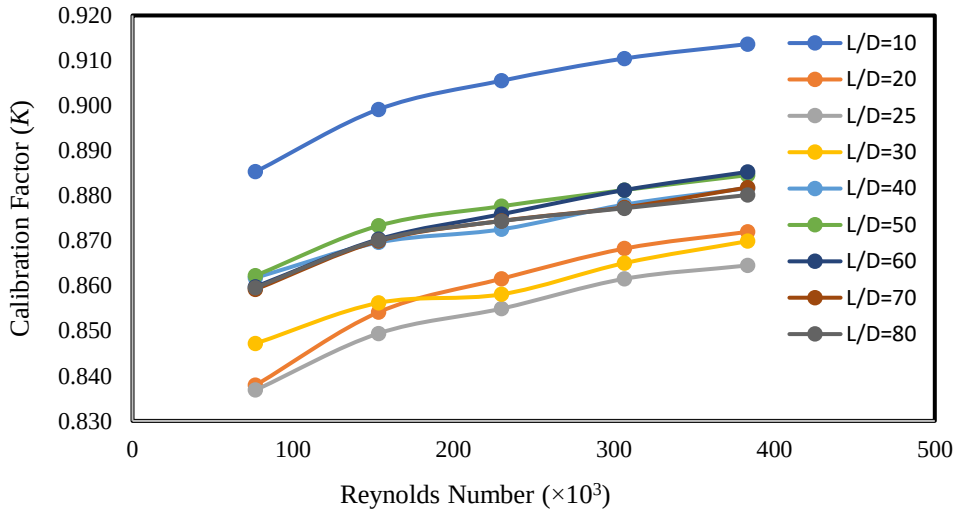

Fig. 7. The calibration factor for the UCCF versus Reynolds number at different upstream lengths. L/D represents normalized upstream pipe length to the pipe diameter

Fig. 8 clearly illustrates the influence of upstream straight pipe length on the required calibration factor for the flowmeter at different fluid Reynolds numbers. Fig. 8 shows that by increasing the normalized upstream straight pipe length (*L/D*), the calibration factor decreases then increase, and finally remains approximately constant. At a distance of about *L/D*=25, the flowmeter requires the lowest calibration factor among the different distances of *L/D*. Moreover, as shown in Fig. 8, at distances farther than *L/D*=40, the flowmeter works independently from the upstream pipe length which provides the suitable conditions for the flowmeter to be installed there. This rise-down behavior of the calibration factor in Fig. 8 could be interpreted according to axial velocity profile evolution through the pipe (Fig. 9) at different locations of the flowmeter.

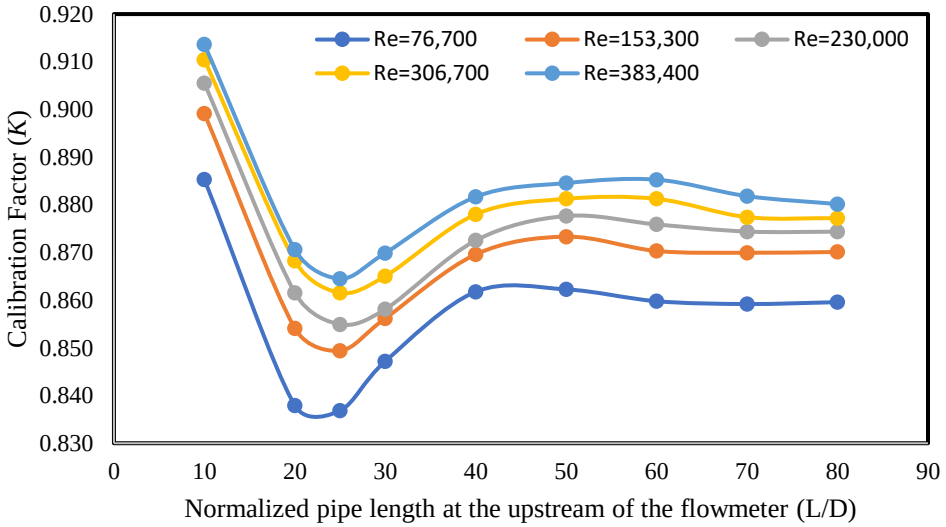

Fig. 8. The influence of the upstream pipe length on the UCCF calibration factor at different flow Reynolds numbers range from 76,700 to 383,400

Fig. 9 shows the axial velocity profile evolution through the pipe at different flow meter locations for the flow, with a Reynolds number of 383,400 as an example. According to Fig. 9, the fluid enters the pipe and moves forward through the pipe; because of shear stress and no-slip condition at the wall, the fuller (or flatter) velocity profile at the pipe entrance tends to become more rounded [1, 19]. The velocity profile evolution continues till the fully-developed length reaches. At distances greater than fully-developed length, the velocity distribution remains fixed in the radial direction [1].

As explained in the numerical validation section, the flowmeter responds to the velocity at the pipe center or mid-section of the pipe. Since the convection velocity computed by the UCCF is intensively dependent on the velocity at the mid-section of the pipe, in a rounded velocity profile, the convection velocity increases relative to average velocity, therefore, the *K* factor decreases (Eq. 3) [1, 12]. In conclusion, in rounded velocity profiles, since the proportion of mid-section velocity to average velocity increases, the calibration factor decreases. On the other hand, in flatter velocity profiles, as the proportion of mid-section velocity to average velocity decreases, the *K* factor increases [1]. This behavior is due to the performance mechanism of the UCCF which is highly sensitive to the velocity at the core region or mid-section of the pipe. With the aid of this argument, the trend of the calibration curve in Fig. 8 could be interpreted.

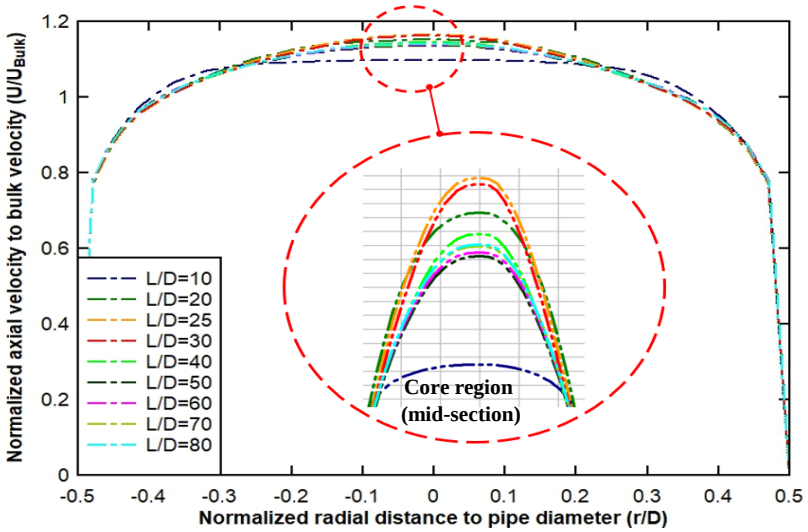

Fig. 9. The dimensionless axial velocity distribution versus dimensionless radius (with focusing on center region or mid-section of the pipe) at various values of upstream length and Re=383,400 as a sample

Explicitly, the area enclosed under the velocity profile stands for the flow rate inside the pipe [19]. However, the velocity profile changes along the pipe length, the enclosed area under each velocity profile, or in other words, the flowrate remains fixed throughout the pipe. Since the flow rate is fixed, accordingly, the bulk velocity (U_{Bulk}) remains constant throughout the pipe [1].

In this regard, the axial velocity distribution in the center of the pipe (core region) at *L/D*=10 is the flattest profile among the axial velocity profiles at different distances of *L/D*. In contrast, at L/D=25, the velocity distribution is the most rounded shape. Carefully noticing the Fig. 9, as the fluid enters the pipe and moves forward inside the pipe, the velocity at the center of the pipe increases till the distance of *L/D*=25 and then decreases till the distance of *L/D*=40 at which the hydrodynamic fully-developed length reaches. Afterward, the core velocity stays approximately constant. The core velocity from *L/D*=40 to *L/D*=80 has nearly the same value. Since the convection velocity ($U_{convection}$) is mainly related to the core region velocity, respecting the argument made above (below Fig. 8) on the core velocity, the following inequality could be concluded for the flow with Re=383,400 as a sample.

$$U_{conv\,@\,\frac{L}{D}=10} < U_{conv\,@\,\frac{L}{D}=40,50,60,70,80} < U_{conv\,@\,\frac{L}{D}=20} < U_{conv\,@\,\frac{L}{D}=30} < U_{conv\,@\,\frac{L}{D}=25} \quad (11)$$

For the flow with a specified Reynolds number (Re=383,400), as discussed above, because the bulk velocity is fixed at various distances of *L/D*, the ratio of the bulk velocity to convection velocity is as follows.

$$\frac{U_{Bulk}}{U_{conv\,@\,\frac{L}{D}=25}} < \frac{U_{Bulk}}{U_{conv\,@\,\frac{L}{D}=30}} < \frac{U_{Bulk}}{U_{conv\,@\,\frac{L}{D}=20}} < \frac{U_{Bulk}}{U_{conv\,@\,\frac{L}{D}=40,50,60,70,80}} < \frac{U_{Bulk}}{U_{conv\,@\,\frac{L}{D}=10}} \quad (12)$$

Consequently, according to the definition of the calibration factor in Eq. 3, the calibration factor inequality at different upstream pipe lengths (*L/D*) is as follows.

$$K_{conv\,@\,\frac{L}{D}=25} < K_{conv\,@\,\frac{L}{D}=30} < K_{conv\,@\,\frac{L}{D}=20} < K_{conv\,@\,\frac{L}{D}=40,50,60,70,80} < K_{conv\,@\,\frac{L}{D}=10} \quad (13)$$

The inequality in Eq. 13 describes exactly the trend shown in Fig. 8 for the flow with Re=383,400 as a sample. For other ranges of the Reynolds number, the same interpretation could be used.

Similarly, to observe the velocity evolution at the core region of the pipe at different distances from *L/D*=10 to *L/D*=80 and various specified Reynolds numbers ranging from 76,600 to 383,400, the maximum velocity across the pipe section as the representative of the core region velocity was plotted in Fig. 10 against the different distances of *L/D*.

Fig. 10 completely conforms to the trend shown in Figs. 8 and 9. Also, lots of numerical and experimental research drew the same trend as shown in Fig. 10 [27–31]. The peak (i.e., an overshoot) in velocity profile evolution shown in Fig. 10, is due to the laminarization tendency of turbulent flow which is mainly related to reversing of streamwise flow along the pipe axis. As the peak occurs in velocity profile development, the streamwise outflow toward the walls follows the streamwise inflow toward the pipe axis. The occurrence of the overshoot phenomenon for turbulent flows was figured out experimentally 45 years ago and it has been further studied [30]. It is out of the scope of the present study to investigate this phenomenon here in detail.

Respecting the discussion in Fig. 9, a similar argument is made here for Fig. 10. As previously explained, as the core region velocity (or maximum velocity) increases, the convection velocity increases, therefore, the calibration factor decreases.

In Fig. 10, the maximum velocity at the core region increases till the distance of *L/D*=20. Correspondingly, the convection velocity which is mainly dependent on the core region velocity (mid-section of the pipe) increases, so to Fig. 8, the *K* factor decrease according to its definition in Eq. 3. As the flow moves forward, the maximum velocity (core region velocity) decreases till the length of *L/D*=40 (Fig. 10), so the convection velocity decreases, therefore, the *K* factor rises to the length of *L/D*=40 as displayed in Fig. 8. For the distances greater than *L/D*=40, since the maximum velocity stays fixed, correspondingly in Fig. 8, the calibration factor remains constant.

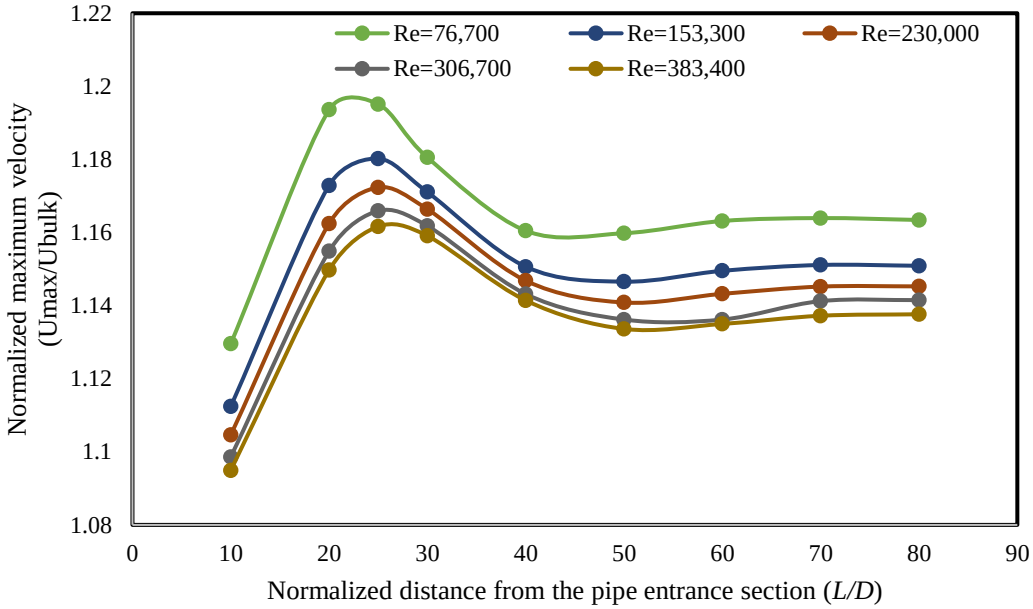

Fig. 10. Normalized maximum velocity across the pipe section at different distances of *L/D* (or different straight pipe lengths the upstream of the flowmeter) for various Reynolds numbers ranging from 76,600 to 383,400

Since the velocity profile develops along the pipe, mounting the flowmeter at various locations observes different velocity distribution that leads to various results. In industrial plants, because of piping limitations, the flowmeter is not mounted at an ideal location every time with relatively long enough upstream straight pipe length (mainly greater than fully-developed length) [1]. Dependency of the flowmeter performance on the position of the flowmeter raises the necessity of using a location-based or in-situ calibration curve [16]. A specific curve of calibration factor for each location of the flowmeter on the pipe is not provided by the manufacturer. To the knowledge of the authors, the manufacturer usually just provides a unique calibration curve for the flowmeter with consideration of sufficiently long upstream straight pipe. To use the manufacturer's unique calibration curve at different flowmeter locations, a correction curve is highly required to modify the manufacturer's unique calibration curve. Therefore, in the present study, as illustrated in Fig. 11a, a correction curve has been provided for the UCCF at different upstream pipe lengths (different locations) and different values of flow Reynolds number to modify the calibration curve at different upstream pipe lengths.

Consequently, for the above explanations, a unique calibration curve could be provided by the flowmeter manufacturer for the flowmeter where the flowmeter upstream pipe length is sufficiently long (mainly greater than the fully-developed length). Afterward, the correction curve in Fig. 11a could modify the calibration curve concerning flowmeter re-position. The

calibration factor (K) should be multiplied by the correction factor (C_r) to account for the influence of upstream straight pipe length.

Therefore, unique calibration curve applicability for the flowmeter (provided by the manufacturer) develops to the distances especially lower than fully-developed length, by the implementation of correction factor on it.

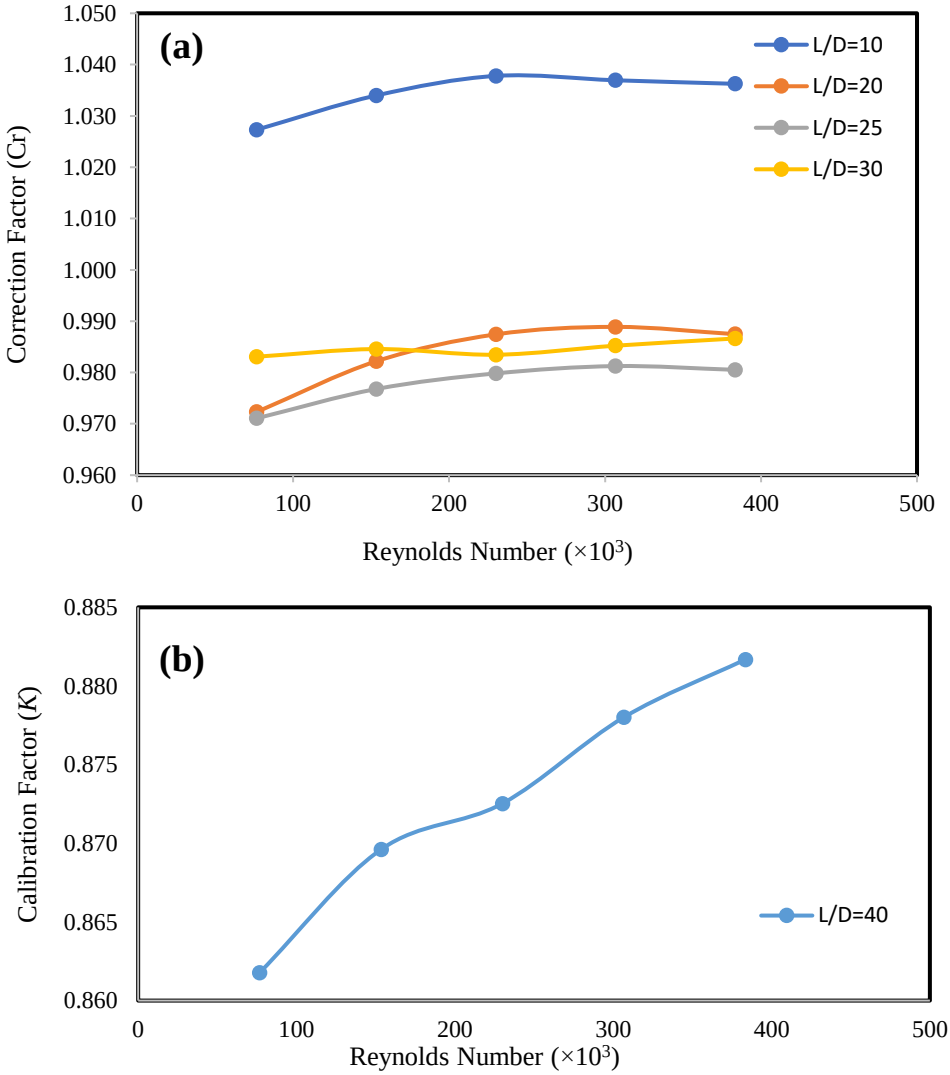

Fig. 11. **(a)** The correction factor versus Reynolds number for the ultrasonic cross-correlation flowmeter at different flowmeter positions. This curve should be implemented on a unique calibration curve. *L/D* represents normalized upstream pipe length to the pipe diameter. **(b)** Unique calculated calibration curve for the flowmeter at the distance of *L/D*=40 (fully-developed length)

It is essential to mention that respecting the results in Figs. 8 and 9, since the flow reaches the fully-developed length at *L/D*=40 and the calibration factor stays approximately fixed at the heights greater than *L/D*=40, the distance of *L/D*=40 (fully-developed length) was considered as a reference location for the preparation of a unique calibration curve. Reference means that the calibration curve for the flowmeter is provided for the *L/D*=40, then other lengths of *L/D* are obtained based on this calibration curve using the correction curve. As mentioned previously, from the authors' experience, the manufacturers also use the fully-developed length to establish predictable and reproducible flow profiles for the preparation of calibration factors.

A sample of the manufacturer's calibration curve was displayed in Fig. 12. Therefore, the required correction factors shown in Fig. 11a should be implemented on the calculated calibration curve for the length of L/D=40, shown in Fig. 11b. For the lengths greater than L/D=40, since the calibration factor remains constant (Fig. 8), the correction factor will be equal to 1, and no correction factor is required for lengths greater than fully-developed length.

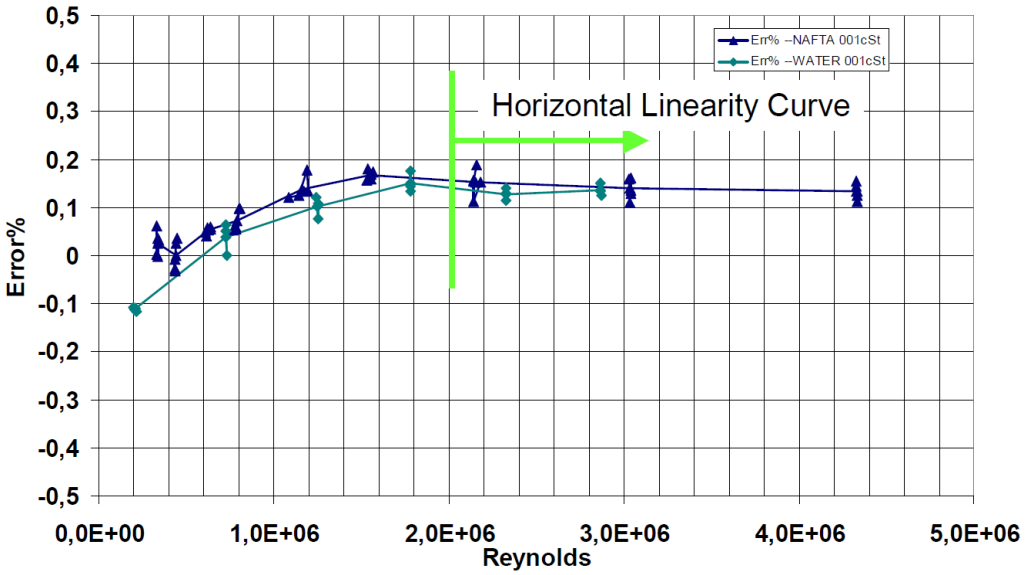

Fig. 12. A sample of the manufacturer's calibration curve for water and naphtha fluids (it belongs to KROHNE company) [32]

Conclusion

In the case of a straight pipe without any flow disturbances (e.g., valve, fitting, and bend) upstream of the flowmeter, the length of the straight pipe, singly, is counted as a critical parameter that highly affects the flowmeter accuracy.

When the flow enters the pipe, the velocity distribution develops along the pipe axis. Installation of the flowmeter at different locations or equally at different upstream pipe lengths, causes the flowmeter to observe different velocity profiles which leads to different measurement results. Therefore, in such conditions, the flowmeter precision is strongly dependable on the upstream straight pipe length. The provision of a proper calibration factor with consideration of the upstream straight pipe length could significantly improve the flowmeter precision.

In this study, using CFD simulations, the water flow inside the straight pipe without any upstream flow disturbances was simulated to study the influence of upstream straight pipe length on the calibration factor for the ultrasonic cross-correlation flowmeter at various Reynolds numbers ranging from 76,600 to 383,400. The results indicated that by increasing the upstream straight pipe length (L) up to the length of approximately 25 times pipe diameter (25D), the required calibration factor decreases sharply, then increases and eventually stays approximately constant at lengths greater than L/D=40, where the fully-developed length reaches. This rise-down trend is due to the velocity profile development along the pipe length. At distances farther than fully-developed length, the flowmeter works independently from the upstream straight pipe length which provides the suitable condition for the flowmeter to be installed there.

Since the flowmeter accuracy changes at different upstream pipe lengths, a correction factor on the calibration curve was finally introduced in the present study in terms of upstream straight pipe length and Reynolds number in order to modify the calibration curve at different upstream pipe lengths.

Nomenclature

Cr	Correction Factor
c_0	Speed of sound (m/s)
D	Pipe diameter (m)
f	Frequency (1/s)
f_e	Characteristic frequency of eddies (1/s)
K	Calibration factor (-)
k	Turbulent kinetic energy (m^2/s^2)
L_{11}	Turbulence longitudinal integral length scale (m)
L	Upstream straight pipe length (m).
p	Pressure (Pa)
q_V	Flowrate (m^3/s)
r	Radial distance (m)
Re	Reynolds Number (-)
u_i	mean (time-average) velocity
X	Upstream signal (rad)
y	Diametrically distance up to pipe diameter (m)
Greek Symbols	
ε	Turbulent dissipation rate (m^2/s^3)
ρ	Density (kg/m^3)
τ	Timeshift (s)
τ^*	Delay time (s)
v	Root mean square velocity (m/s)
ϕ	Signal phase angle (rad)
ω_0	Acoustic beam frequency (rad/s)
Δx	Sensors separation spacing (m)
ε	Turbulent dissipation rate (m^2/s^3)
ρ	Density (kg/m^3)
Subscripts	
T	Measurement Time (s)
t	Time (s)
U	Mean axial velocity (m/s)
$U_{convection}$	Convection velocity (m/s)
u_i'	Velocity fluctuation (m/s)
V	Volumetric
i	x_i cartesian direction
0	Relates to Ultrasonic beam
*	Relates to UCCF measured time

References

[1] Alaeddin MA, Mousavi SF, Hashemabadi SH. Numerical study on the effect of circumferential position of ultrasonic transducers on ultrasonic cross-correlation flowmeter performance under asymmetric airflow profile. Ultrasonics. 2021;115:106479.

[2] Mousavi SF, Hashemabadi SH, Jamali J. Calculation of geometric flow profile correction factor for ultrasonic flow meter using semi-3D simulation technique. Ultrasonics. 2020;106:106165.
[3] LaNasa PJ, Upp EL. Liquid Flow Measurement. Second ed. Florida: Gulf Professional Publishing; 2002.
[4] Lynnworth LC, Liu Y. Ultrasonic flowmeters: Half-century progress report, 1955-2005. Ultrasonics. 2006;44.
[5] Zhou H, Ji T, Wang R, Ge X, Tang X, Tang S. Multipath ultrasonic gas flowmeter based on multiple reference waves. Ultrasonics. 2018;82:145–52.
[6] Coulthard J. Ultrasonic cross-correlation flowmeters. Ultrasonics. 1973;11(2):83–8.
[7] Schneider F, Peters F, Merzkirch W. Quantitative analysis of the cross-correlation ultrasonic flow meter by means of system theory. Measurment Science and Technology. 2003;14(5):573–82.
[8] Worch A. A clamp-on ultrasonic cross correlation flow meter for one-phase flow. Measurment Science and Technology. 1998;9(4):622–30.
[9] Fernandes CW, Bellar MD, Werneck MM. Cross-correlation-based optical flowmeter. IEEE Transactions on Instrumentation and Measurement. 2010;59(4):840–6.
[10] Beck MS. Correlation in instruments: cross correlation flowmeters. Journal of Physics E: Scientific Instruments. 1981;14(1):7.
[11] Lysak PD, Jenkins DM, Capone DE, Brown WL. Analytical model of an ultrasonic cross-correlation flow meter, part 1: Stochastic modeling of turbulence. Flow Measurment and Instrumentation. 2008;19(1):1–7.
[12] Lysak PD, Jenkins DM, Capone DE, Brown WL. Analytical model of an ultrasonic cross-correlation flow meter, part 2: Application. Flow Measurment and Instrumentation. 2008;19(1):41–6.
[13] Gurevich AY, Goman MG, Gurevich YG, Lopez AM. Synthetic turbulence modeling for evaluation of ultrasonic cross-correlation flow measurement. Flow Measurment and Instrumentation. 2018;60:134–43.
[14] Wada S, Tezuka K, Treenuson W, Tsuzuki N, Kikura H. Study on the optimal number of transducers for pipe flow rate measurement downstream of a single elbow using the ultrasonic velocity profile method. Science and Technology of Nuclear Installations. 2012.
[15] American Petroleum Institute. Manual of Petroleum Measurement Standards Chapter 5.8, Measurement of Liquid Hydrocarbons by Ultrasonic Flow Meters. API MPMS 5.8. 1994.
[16] International Organization for Standardization. Measurement of fluid flow in closed conduits Ultrasonic transit-time meters for liquid. ISO 12242. 2012.
[17] Zhao H, Peng L, Takahashi T, Hayashi T, Shimizu K, Yamamoto T. ANN based data integration for multi-path ultrasonic flowmeter. IEEE Sensors journal. 2014;14(2):362–70.
[18] Ton V. A mathematical model of ultrasonic cross correlation flow meters based on industrial experience. Flow Measurment and Instrumentation. 2020;75:101775.
[19] Cengel Y, Cimbala J. Essentials of Fluid Mechanics: Fundamentals and Applications. Fourth ed. New York: McGraw-Hill Education; 2008.
[20] Bird RB, Stewart WE, Lightfoot EN. Transport phenomena. Second ed. Vol. 1. New York: John Wiley & Sons; 2006.
[21] Pollard A, Martinuzzi R. Comparative study of turbulence models in predicting turbulent pipe flow. II - Reynolds stress and k-epsilon models, AIAA journal. 27 (1989) 1714–1721.
[22] Loyseau X.F, Verdin P.G, Brown L.D. Scale-up and turbulence modelling in pipes, Journal of Petroleum Science and Engineering. 162 (2018) 1–11.
[23] Kalpakli Vester A, Orlu R, Alfredsson P.H. Turbulent flows in curved pipes: Recent advances in experiments and simulations, Applied Mechanics Reviews. 68 (2016).
[24] Lysak PD, Brungart TA. Velocity spectrum model for turbulence ingestion noise from computational-fluid-dynamics calculations. AIAA Journal. 2003;41(9):1827–9.
[25] National Iranian Oil and Engineering Company. NIOEC specification for design criteria for process and mechanics. NIOEC-SP-00-50. 2006.
[26] Zhao H, Peng L, Stephane SA, Ishikawa H, Shimizu K, Takamoto M. CFD aided investigation of multipath ultrasonic gas flow meter performance under complex flow profile. IEEE Sensors Journal. 2014;14(3):897–907.
[27] Anselmet F, Ternat F, Amielh M, Boiron O, Boyer P, Pietri L. Axial development of the mean

flow in the entrance region of turbulent pipe and duct flows. Comptes Rendus Mécanique. 2009;337(8):573–84.
[28] Duz H. Numerical Flow Analysis of The Variation of Central Axial Velocity Along The Pipe Inlet. The Eurasia Proceedings of Science Technology Engineering and Mathematics. 2018;2:323–33.
[29] Martins RS, Ramos R. Numerical evaluation of upstream bend installation effects on fully developed flow profiles aiming ultrasonic flow metering. 21st International Congress of Mechanical Engineering Outubro. 2011.
[30] Bryant DB, Sparrow EM, Gorman JM. Turbulent pipe flow in the presence of centerline velocity overshoot and wall-shear undershoot. International Journal of Thermal Sciences. 2018;125:218–30.
[31] Kumara WAS, Halvorsen BM, Melaaen MC. Computational study on non-asymptotic behavior of developing turbulent pipe flow. Advances in Fluid Mechanics VIII. 2010. p. 39–53.
[32] Hogendoorn J, Boer A.Ž, Danen H. An ultrasonic flowmeter for custody transfer measurement of LNG: A challenge for design and calibration. 25 th International North Sea Flow Measurement Workshop. 2007; 350–365.

How to cite: Alaeddin MA, SH Hashemabad. CFD Study of Calibration Factor for Cross Correlation Based Ultrasonic Flowmeter at Different Upstream Pipe Lengths. Journal of Chemical and Petroleum Engineering. 2022; 56(1): 133-152.